5
Combustion of Crystalline and Polymeric Materials

5.1
Combustion of Crystalline Materials

5.1.1
Ammonium Perchlorate (AP)

5.1.1.1 Thermal Decomposition

Experimental studies on the thermal decomposition and combustion processes of AP have been carried out and their detailed mechanisms have been reported.[1–11] Fig. 5.1 shows the thermal decomposition of AP as measured by differential thermal analysis (DTA) and thermal gravimetry (TG) at a heating rate of 0.33 K s^{-1}. An endothermic peak is seen at 520 K, corresponding to an orthorhombic to cubic lattice crystal structure phase transition, the heat of reaction for which amounts to

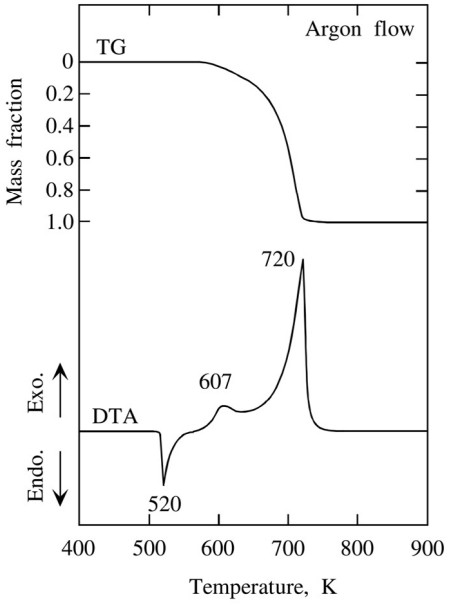

Fig. 5.1 Thermal decomposition process of AP measured by thermal gravimetry (TG) and by differential thermal analysis (DTA).

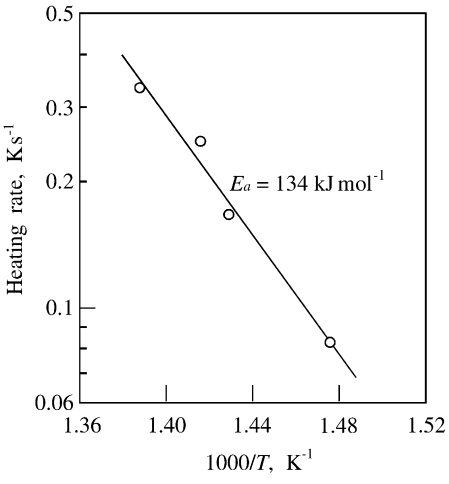

Fig. 5.2 Determination of the activation energy of AP decomposition.

–85 kJ kg^{-1} without mass loss. An exothermic reaction occurs between 607 K and 720 K accompanied by mass loss. This exothermic reaction occurs through the following overall reaction scheme:[1,2]

$$NH_4ClO_4 \rightarrow NH_3 + HClO_4$$
$$HClO_4 \rightarrow HCl + 2O_2$$

This process produces excess oxygen as an oxidizer. The exothermic peak shifts towards higher temperatures as the heating rate is increased. Fig. 5.2 shows that a plot of heating rate versus reciprocal temperature produces a straight line that indicates the activation energy for the exothermic gasification reaction. The activation energy is thereby determined as 134 kJ mol^{-1}. However, the decomposition reaction includes sublimation and melting processes that cannot be identified from the DTA and TG data. Dissociative sublimation occurs when the heating rate is slow compared with the heating rate of normal burning.[5] This sublimation is endothermic by 2.1 MJ kg^{-1} and zeroth order with respect to pressure. Melting of AP occurs in a higher temperature zone, above 725 K, when the heating rate is high.

5.1.1.2 **Burning Rate**

The mode of degradation of AP was first studied by Bircumshaw and Newman.[3] They found that below 570 K only 30% decomposition occurs; the remaining 70% is a porous solid residue chemically identical to the starting AP that does not react further when the pressure and temperature are very low. Above 670 K, no solid residue remains. When the pressure is increased, pure sublimation is suppressed and the decomposition reaction is favored. AP degradation involves dissociative sublimation of a loosely bound $NH_3 \cdot HClO_4$ complex as a first step, liberating gaseous NH_3 and $HClO_4$. The combustion of AP particles is sustained by the heat generated at the burning surface and the transfer back from the gas phase of the

heat produced by the reaction between $HClO_4$ and NH_3 molecules. The gas-phase reaction is a second-order process and the adiabatic flame temperature is 1205 K.

The burning rate of a pressed strand of AP as a function of pressure has been dealt with by Arden[1] and by Levy and Friedman.[2] The lower pressure limit of AP burning is about 2.7 MPa and the burning rate increases as the pressure is increased above this lower limit. The thickness of the gas-phase reaction of NH_3/$HClO_4$ is less than 100 μm at 10 MPa and decreases as the pressure is increased, and the reaction time is inversely proportional to the pressure (MPa) represented by $6.5 \times 10^{-7}/p$ seconds.[8]

5.1.1.3 Combustion Wave Structure

When a pressed strand of AP burns, a high-temperature flame is formed in the gas phase due to the exothermic reaction between NH_3 and $HClO_4$. Mitani and Niioka measured the gas-phase structure above the regressing surface of an AP pellet and found a two-stage flame,[12] and an AP deflagration model has been presented by Guirao and Williams.[13] Heat conducted from the flame to the burning surface is used to heat the solid phase from its initial temperature to the surface temperature. At the burning surface, the AP crystals go through an orthorhombic to cubic lattice transition. This transition is endothermic by 80 kJ kg^{-1} and occurs at about 513 K. Tanaka and Beckstead carried out a computational study of the condensed-phase and gas-phase structures of AP by assuming 107 reaction steps and 32 gaseous species.[14] The burning surface temperature and the melt layer thickness were also computed as a function of pressure. The activation energy of the surface reaction was found to be about 63 kJ mol^{-1} and the pressure exponent of burning rate, n, is around 0.77 between 2.7 MPa and 10 MPa.[14]

5.1.2 Ammonium Nitrate (AN)

5.1.2.1 Thermal Decomposition

AN melts at 443 K and begins to gasify above 480 K. The decomposition process of AN is temperature-dependent. At low temperatures, i. e. around 480 K, the gasification process of AN is the endothermic (–178 kJ mol^{-1}) reversible reaction represented by[15]

$$NH_4NO_3 \rightleftharpoons NH_3 + HNO_3$$

The decomposition process shifts to an exothermic (37 kJ mol^{-1}) gasification reaction as the temperature increases:

$$NH_4NO_3 \rightarrow N_2O + 2H_2O$$

and then the overall decomposition reaction of AN appears to be

$$NH_4NO_3 \rightarrow N_2 + 2H_2O + 1/2O_2$$

This reaction is highly exothermic (119 kJ mol^{-1}) and produces oxygen molecules which act as an oxidizer. Though the ignition of AN is difficult due to the initial endothermic reaction, AN becomes highly inflammable in the high pressure region and also becomes detonable when heated beyond 550 K. Furthermore, the inflammable characteristics of AN are dependent on impurities or additives.

5.1.3 HMX

5.1.3.1 Thermal Decomposition

Very detailed literature accounts and discussions of the thermal decomposition of nitramines such as HMX and RDX have been presented by Boggs,[16] and a general picture of the decomposition processes of nitramines can be gleaned from further references.[15–24] When HMX is slowly heated, a single-stage mass-loss process is observed:[17] the mass loss begins at 550 K and a rapid gasification reaction occurs at 553 K. No solid residue remains above 553 K. Two endothermic peaks and one exothermic peak are seen: the first endothermic peak at 463 K corresponds to the crystal transformation from β to δ and the second endothermic peak at 550 K corresponds to the phase change from solid to liquid. The exothermic peak at 553 K is caused by the reaction and the accompanying gas-phase reaction.

A thermally degraded HMX sample, as obtained by decomposition interrupted at the 50 % mass-loss condition (the heating is stopped at 552 K and the sample is cooled to room temperature, 293 K) is identified as a recrystallized material.[17] Gasification of the thermally degraded HMX begins at 550 K and rapid decomposition occurs at 553 K, which is equivalent to the thermal decomposition process of non-degraded HMX. However, the endothermic peak observed at 463 K is not seen for the degraded HMX. The results of an infrared (IR) analysis of β-HMX, δ-HMX, and the degraded HMX show that the degraded HMX is equivalent to δ-HMX, which implies that the endothermic process of the phase change from solid to liquid observed at 550 K can be ascribed to δ-HMX.

5.1.3.2 Burning Rate

Since HMX is composed of fine, crystalline particles, it is difficult to measure its linear burning rate. When a large-sized HMX single crystal (approximately 10 mm × 10 mm × 20 mm) is ignited by means of an electrically heated wire attached to the top of the crystal, the crystal immediately breaks into fragments following ignition because of the thermal stress created therein. As a result, no steady burning of the crystal is possible, and no linear burning rate exists for HMX because the heat conduction rate from the ignited surface to the interior of the crystal is faster than the surface regressing rate (burning rate). A breakage of the HMX crystal structure occurs due to the thermal stress caused by the temperature difference in the crystal.

When a pressed pellet made of HMX particles is ignited from the top, it burns steadily without breakage of the pellet. The thermal stress created within the pressed pellet is dissipated at the interfaces of the HMX particles within the pellet. Furthermore, the density of the pressed pellet is at most 95 % of the theoretical HMX den-

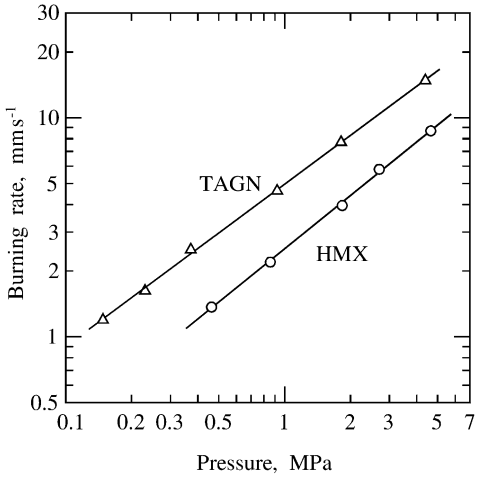

Fig. 5.3 Burning rates of HMX and TAGN showing that the burning rate of HMX is lower than that of TAGN.

sity and the thermal stress imparted to the crystal is absorbed by the voids between the HMX particles. The burning rate of an HMX sample pressed into pellet form is shown in Fig. 5.3. The pressed pellet is composed of a mixture of β-HMX particles of 20 μm in diameter (33 %) and 200 μm in diameter (67 %). The pellets have dimensions of diameter 8 mm and length 7 mm and their density is 1700 kg m^{-3}, which is 89 % of the theoretical maximum density (1900 kg m^{-3}). The burning rate of the HMX pellets is seen to increase linearly in an ln r versus ln p plot. The pressure exponent of the burning rate is 0.66 at an initial temperature of 293 K.

5.1.3.3 **Gas-Phase Reaction**

The overall initial decomposition reaction of HMX is represented by[18,19]

$$3(CH_2NNO_2)_4 \rightarrow 4NO_2 + 4N_2O + 6N_2 + 12CH_2O$$

Since nitrogen dioxide reacts quite rapidly with formaldehyde,[16,20,25] the gas-phase reaction represented by

$$7NO_2 + 5CH_2O \rightarrow 7NO + 3CO + 2CO_2 + 5H_2O$$

is probably the dominating reaction immediately after the initial decomposition reaction. The reaction between NO_2 and CH_2O is highly exothermic and the reaction rate is faster than the reaction rates of the other gaseous species.

The products generated by the above reactions react again at a later stage, i. e., NO and N_2O act as oxidizers, and H_2 and CO act as fuels. The reactions involving NO and N_2O are represented by[25]

$$2NO + 2H_2 \rightarrow N_2 + 2H_2O$$
$$2NO + 2CO \rightarrow N_2 + 2CO_2$$
$$2N_2O \rightarrow 2NO + N_2$$

The overall reactions involving NO and N_2O take place slowly and are trimolecular,[25] hence the reaction rate is very slow at low pressure and increases rapidly as the pressure is increased.

5.1.3.4 Combustion Wave Structure and Heat Transfer

Typical flame structures of HMX pellets as a function of pressure are shown in Fig. 5.4. A thin luminous flame sheet stands some distance from the burning surface and a reddish flame is produced above this luminous flame sheet. The flame sheet approaches the burning surface as the pressure is increased.[17] When the pressure is less than 0.18 MPa, the luminous flame sheet is blown off from the burning surface as shown in Fig. 5.4 (a). As the pressure is increased, the luminous flame sheet rapidly approaches the burning surface. However, the luminous flame sheet becomes very unstable above the burning surface and forms a wave-shaped flame sheet in the pressure range between 0.18 MPa and 0.3 MPa, as shown in Fig. 5.4 (b). On further increasing the pressure above 0.3 MPa, the luminous flame sheet becomes stable and one-dimensional in shape, just above the burning surface, as shown in Fig. 5.4 (c).

The combustion wave of HMX is divided into three zones: crystallized solid phase (zone I), solid and/or liquid condensed phase (zone II), and gas phase (zone III). A schematic representation of the heat transfer process in the combustion wave is shown in Fig. 5.5. In zone I, the temperature increases from the initial value T_0 to the decomposition temperature T_u without reaction. In zone II, the temperature increases from T_u to the burning surface temperature T_s (interface of the condensed phase and the gas phase). In zone III, the temperature increases rapidly from T_s to the luminous flame temperature (that of the flame sheet shown in Fig. 5.4). Since the condensed-phase reaction zone is very thin (~ 0.1 mm), T_s is approximately equal to T_u.

The heat flux transferred back from zone III to zone II, Λ_{III}, is given by

$$\Lambda_{III} = \lambda_{III}(dT/dx)_{III} \tag{5.1}$$

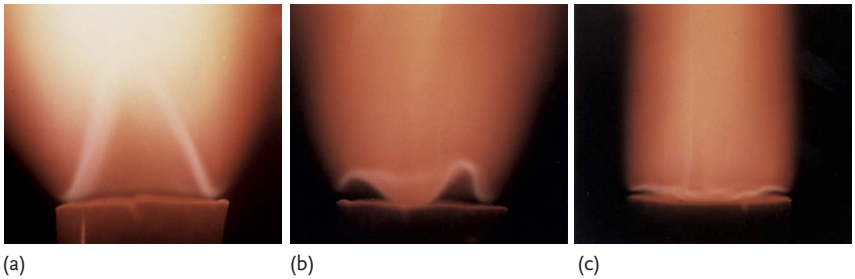

(a) (b) (c)

Fig. 5.4 Flame photographs of HMX at three different pressures: (a) 0.18 MPa, (b) 0.25 MPa, and (c) 0.30 MPa.

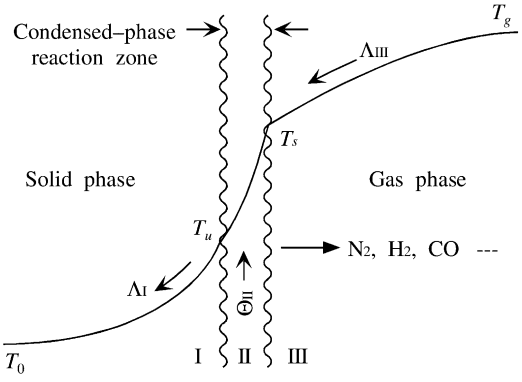

Fig. 5.5 Heat transfer model of the combustion wave of an energetic material.

and the heat flux produced in zone II, Θ_{II}, is given by

$$\Theta_{II} = \rho_I \, r \, Q_{II} \tag{5.2}$$

where Q_{II} is the heat of reaction in zone II. The heat balance equation at the burning surface is represented by

$$\Theta_{II} = \rho_I \, r \, c_I \, (T_s - T_0) - \Lambda_{III} \tag{5.3}$$

The temperature gradient in zone III, $(dT/dx)_{III}$, increases as the pressure is increased, according to $(dT/dx)_{III} \sim p^{0.7}$. However, T_s remains relatively constant (~ 700 K) in the pressure range between 0.1 MPa and 0.5 MPa. Using the physical parameter values of HMX, $\rho_I = 1700$ kg m^{-3}, $c_I = 1.30$ kJ kg^{-1} K^{-1}, and $\lambda_{III} = 8.4 \times 10^{-5}$ kW m^{-1} K^{-1}, Q_{II} is determined as 300 kJ kg^{-1}.

Fig. 5.6 shows the heat flux produced in zone II and the heat flux transferred back from zone III to zone II as a function of pressure. Θ_{II} is approximately equal to Λ_{III}, both of which increase with increasing pressure according to $\Lambda_{III} \sim p^{0.75}$ and $\Theta_{II} \sim p^{0.65}$. It is evident from Eq. (5.2) that the pressure sensitivity of Θ_{II} is approximately equal to that of the burning rate. The pressure sensitivity of the HMX burning rate ($\sim p^{0.66}$) is therefore dependent on Λ_{III}, i. e., the pressure sensitivity of the gas-phase reaction.[17]

5.1.4
Triaminoguanidine Nitrate (TAGN)

5.1.4.1 Thermal Decomposition

The oxidizer fragment (HNO_3) of TAGN is attached by an ionic bond in the molecular structure and the physicochemical processes of TAGN combustion are different from those of HMX and RDX, the oxidizer fragment of which (-N–NO_2) is attached by a covalent bond in their molecular structures. Though the flame temperature of TAGN is lower than that of HMX by 1200 K, the value of the thermodynamic parameter $(T_f/M_g)^{1/2}$ appears to be approximately the same for both materials. The

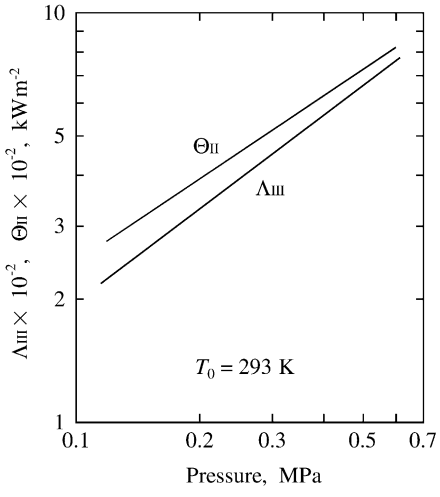

Fig. 5.6 Heat flux transferred back from the gas phase to the burning surface and heat flux produced at the burning surface.

major combustion products of TAGN are N_2, H_2, and H_2O, and those of HMX are N_2, CO, and H_2O. The molecular mass, M_g, of TAGN is 18.76 kg kmol^{-1} and that of HMX is 24.24 kg kmol^{-1}. TAGN produces a high concentration of hydrogen gas, which increases the value of the thermodynamic parameter even though the flame temperature is low.

Fig. 5.7 shows scanning electron microphotographs of a TAGN surface before combustion (a) and after quenching (b). The quenched surface is prepared by a rapid pressure decay in the strand burner shown in Appendix B. The quenched sur-

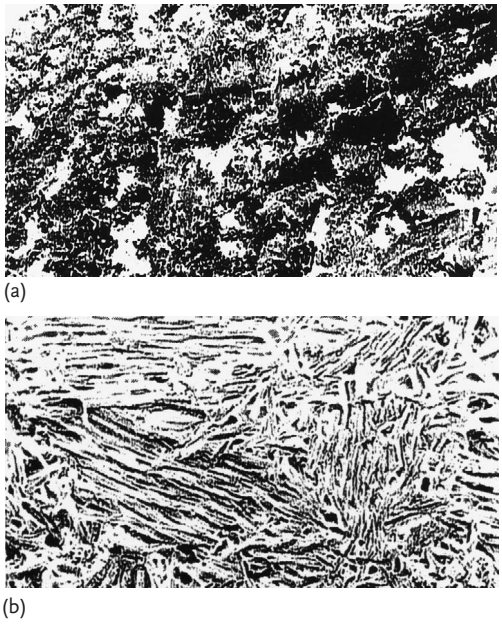

Fig. 5.7 Scanning electron microphotographs of a TAGN surface before combustion (a) and after quenching (b) from the burning pressure of 1.0 MPa.

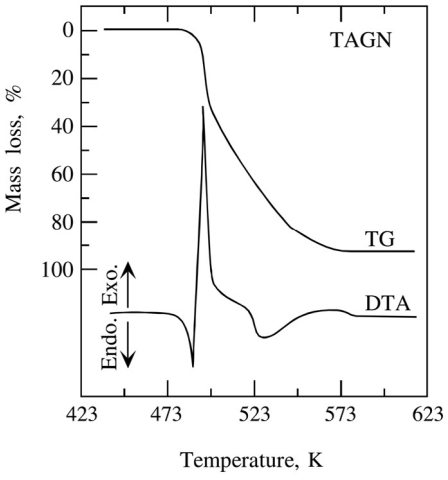

Fig. 5.8 DTA and TG results for TAGN showing a rapid exothermic reaction in the first stage of the decomposition process.

face shows finely divided recrystallized material dispersed homogeneously over it. It is evident that TAGN forms a melted layer and then decomposes to produce reactive gaseous species at the burning surface during burning.

The thermal decomposition of TAGN consists of a three-stage heat generation and mass loss process when measured by means of differential thermal analysis(DTA) and thermogravimetry (TG), as shown in Fig. 5.8.[26] The first stage corresponds to the rapid exothermic reaction between mass losses of 0% (488 K) and 27% (498 K), the second stage corresponds to the relatively slow endothermic reaction between mass losses of 27% (498 K) and 92% (573 K), and the third stage corresponds to the very slow endothermic reaction between mass losses of 92% (573 K) and 100% (623 K). The endothermic peak at 488 K corresponds to the phase change from solid to liquid. The exothermic rapid reaction in the first stage is the process representing the nature of the energetics of TAGN. This exothermic reaction occurs immediately after the endothermic phase change.

Thermally treated TAGN, as obtained by interrupted decomposition at 27% mass loss, decomposes without the exothermic peak observed as the first stage for TAGN. As shown in Fig. 5.9 (dotted lines), the gasification reaction starts at 498 K and the main decomposition reaction is complete at about 553 K. The exothermic peak observed as the first stage of the TAGN decomposition process shown in Fig. 5.8 is completely absent. This indicates that the main energetic fragment of TAGN is used up in the first stage of the decomposition reaction, accompanied by the 27% mass loss.

The molecular structure of guanidine nitrate (GN: $CH_6N_4O_3$) is similar to that of TAGN, except that the latter has three additional amino groups:

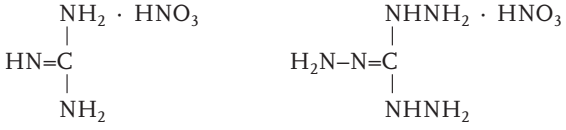

Molecular structure of GN Molecular structure of TAGN

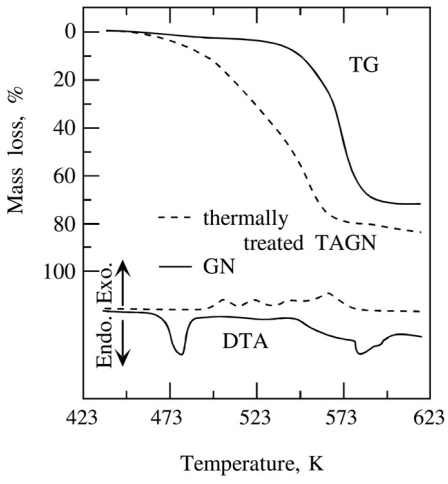

Fig. 5.9 DTA and TG results for a thermally treated TAGN and for GN, showing the lower energetic nature of both materials.

The results of DTA and TG of GN are shown in Fig. 5.9 (solid lines). The endothermic peak at 483 K corresponds to the phase change from solid to liquid and a very slow reaction occurs after this phase change. The main decomposition of GN begins at about 530 K and is complete at 539 K (70 % mass loss). The remaining 30 % mass fragment decomposes endothermically at higher temperatures. Although GN is also an energetic material (T_f = 1370 K and ΔH_f = –3.19 MJ kg^{-1}) consisting of an oxidizer fragment (HNO_3) attached by an ionic bond and fuel fragments, neither a rapid gasification reaction nor an exothermic reaction occurs. This is a significant contrast in comparison with the decomposition process of TAGN. Thus, one can conclude that the HNO_3 moiety attached to the molecular structure of TAGN is not the fragment responsible for the exothermic rapid reaction in the first stage of the decomposition process.[26]

Fig. 5.10 shows the infrared spectra of TAGN, thermally treated TAGN, and GN. It is evident that the -NH_2 and -C–N bonds of TAGN disappear almost completely when it is thermally treated until the exothermic peak occurs (27 % mass loss). The spectrum of the thermally treated TAGN is similar to that of GN. Through the C–N bond breakage, liquefied gaseous fragments are formed; the –NH_2 bond of TAGN is no longer present in thermally treated TAGN. This implies that N–NH_2 bond breakage occurs, liberating NH_2 fragments in the first stage of the decomposition. Since the weakest chemical bond in the TAGN molecule is the N–N bond (159 kJ mol^{-1}), the initial bond breakage cleaves the amino groups. The NH_2 radicals attached to the TAGN molecule are split off. The mass fraction of 3(NH_2) within the TAGN molecule is 0.288, which is approximately equal to the observed mass loss fraction (0.27) in the first stage of the decomposition process. The chemical enthalpy difference between TAGN and GN is 344 kJ mol^{-1}, and the energy released by the reaction of NH_2 radicals to produce N_2 and H_2 is 168 kJ mol^{-1}.[26] This energy is the heat produced in the first stage of the decomposition process of TAGN.

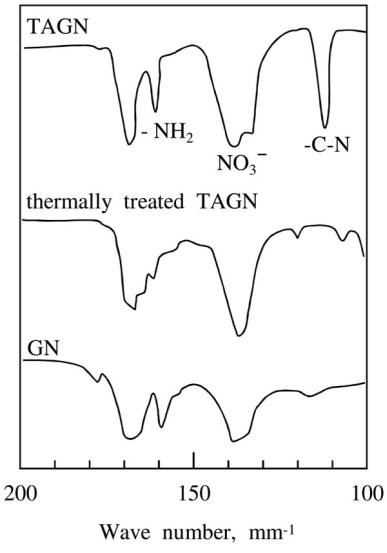

Fig. 5.10 Infrared spectra of TAGN, thermally treated TAGN, and GN.

5.1.4.2 **Burning Rate**

Since TAGN is composed of crystalline particles, its burning rate is measured using pressed pellets. The burning rate of TAGN as a function of pressure is shown in Fig. 5.3. Each pressed pellet is made from TAGN particles 5 μm in diameter and has a density of 1470 kg m^{-3}, which is 98 % of the theoretical maximum density. The burning rate is seen to increase linearly in an ln r versus ln p plot and the pressure exponent n is 0.78, which is equivalent to the pressure exponent of HMX, as is also shown in Fig. 5.3 as a reference.[21] The burning rate of TAGN is almost double that of HMX at the same pressure, even though its energy density is lower than that of HMX, as shown in Table 2.7.

5.1.4.3 **Combustion Wave Structure and Heat Transfer**

Fig. 5.11 shows a flame photograph of TAGN burning at 0.2 MPa. The luminous flame of TAGN stands some distance from the burning surface, but the luminous flame front approaches the burning surface when the pressure is increased, similarly to the luminous flame of HMX described in Section 5.1.3. As for double-base propellants and nitramines, the flame stand-off distance is represented by

$$L_g = ap^d \tag{5.4}$$

where d is –1.00. In an analysis based on Eq. (3.70), the overall reaction rate in the gas phase, $[\omega_g]$, can be expressed as:

$$[\omega_g] = \rho pr/L_g \tag{5.5}$$

$$\sim p^{m-d} \sim p^m \tag{5.6}$$

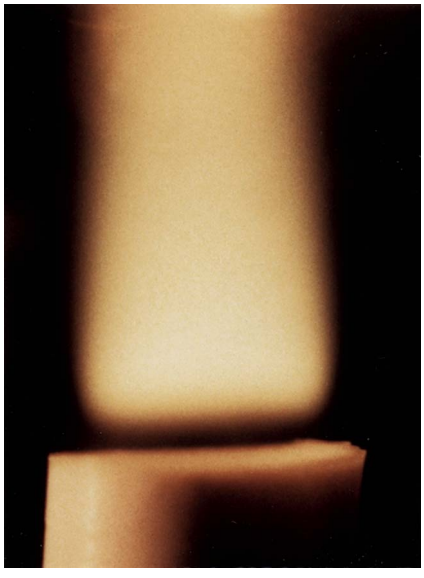

Fig. 5.11 Flame structure of TAGN showing a luminous flame standing above the burning surface: the flame front approaches the burning surface as the pressure is increased (not shown).

The reaction rate is seen to increase linearly in an ln $[\omega_g]$ versus ln p plot, and the overall order of the reaction in the gas phase is determined to be $m = 1.78$ based on the relationship $m = n - d$. This indicates that the reaction rate of TAGN in the gas phase is less pressure-sensitive than that of nitropolymer propellants; for example, $m = 2.5$ for double-base propellants.[26]

The heat transfer process in the combustion wave of TAGN consists of three zones, similar to what was illustrated for HMX in Fig. 5.5. Zone I is the solid phase, the temperature of which increases exponentially from the initial temperature, T_0, to the decomposition temperature, T_u, without chemical reaction. Zone II is the condensed phase, the temperature of which increases from T_u to the burning surface temperature, T_s, in an exothermic reaction. Zone III is the gas phase, the temperature of which increases rapidly from T_s to the final combustion temperature, T_g, in an exothermic reaction.

Fig. 5.12 shows the result of a measurement of the temperature profile in the combustion wave of TAGN. The melt layer temperature T_u is about 750 K and T_s is about 950 K, both of which remain relatively unchanged when the pressure is increased. Both the thickness of the condensed-phase reaction zone II and the heat flux feedback from zone III to zone II, Λ_{III}, increase as the pressure is increased, as shown in Fig. 5.13. At 0.3 MPa, the heat flux in zone II, Θ_{II}, is approximately 13 times higher than that in zone III, Λ_{III}, as shown in Fig. 5.14. The heat of reaction in zone II, Q_{II}, is determined to be 525 kJ kg^{-1}. It is evident that Q_{II} of TAGN is approximately 75 % higher than Q_{II} of HMX. Thus, the higher burning rate of TAGN compared to that of HMX shown in Fig. 5.3 is caused by the higher Q_{II} of TAGN, even though the adiabatic flame temperature of TAGN is about 1200 K lower than that of HMX. The decomposition and combustion of TAGN are discussed in detail in a symposium report.[26]

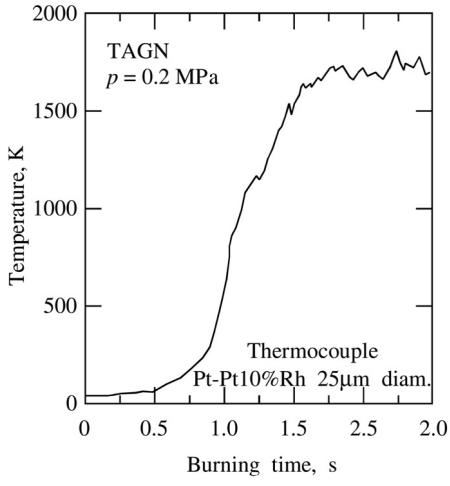

Fig. 5.12 Temperature profile in the combustion wave of TAGN.

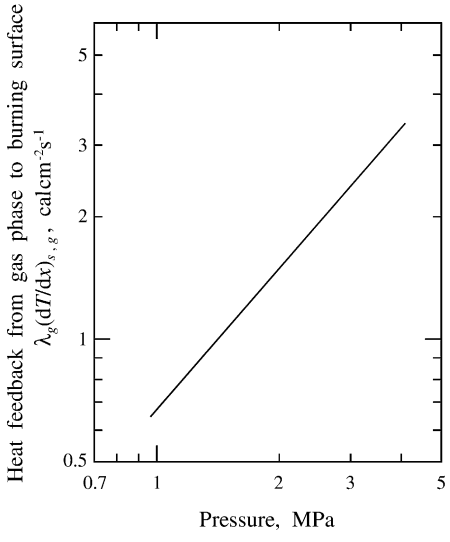

Fig. 5.13 Heat flux transferred back from the gas phase to the burning surface of TAGN.

5.1.5
ADN (Ammonium Dinitramide)

DSC and DTA measurements show melting of ADN, $NH_4N(NO_2)_2$, at 328 K, the onset of decomposition at 421 K, and an exothermic peak at 457 K.[27] Gasification of 30% of the mass of ADN occurs below the exothermic peak temperature, and the remaining 70% decomposes after the peak temperature. The decomposition is initiated by dissociation into ammonia and hydrogen dinitramide. The hydrogen dinitramide further decomposes to ammonium nitrate and N_2O. The final decomposition products in the temperature range 400–500 K are NH_3, H_2O, NO,

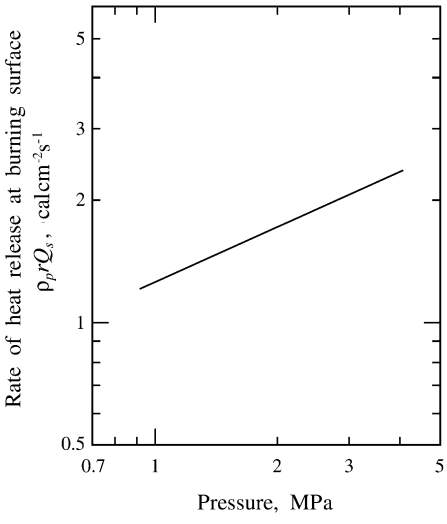

Fig. 5.14 Rate of heat release at the burning surface of TAGN as a function of pressure.

N_2O, NO_2, HONO, and HNO_3, with a total heat release of approximately 240 kJ mol^{-1}.[28] These molecules react in the gas phase to form O_2, H_2O, and N_2 as the final combustion products and the adiabatic flame temperature reaches 3640 K. The excess oxygen molecules act as an oxidizer when ADN is mixed with fuel components.

The combustion wave structure of ADN consists of three zones: the melt layer zone, the preparation zone, and the flame zone. The temperature remains relatively unchanged in the melt layer zone, then increases rapidly just above the melt layer zone to form the preparation zone, in which it rises from about 1300 to 1400 K. At some distance above the melt layer zone, the temperature increases rapidly to form the flame zone, in which the final combustion products are formed.

Similar to the situation with nitrate esters, the two-stage gas-phase reaction resulting from the combustion of ADN occurs due to the reduction of NO to N_2, which is reported to be a termolecular reaction. The heat flux transferred back from the preparation zone to the melt layer zone dominates the gasification process occurring in the melt layer zone.

5.1.6
HNF (Hydrazinium Nitroformate)

HNF, $N_2H_5C(NO_2)_3$, melts at 397 K and completely decomposes at 439 K, accompanied by an energy release of 113 kJ mol^{-1}. DTA and TG analyses reveal that the thermal decomposition of HNF occurs in two steps. The first step is an exothermic reaction accompanied by 60 % mass loss in the temperature range 389–409 K. The second step is another exothermic reaction accompanied by 30 % mass loss in the temperature range 409–439 K. These two steps occur successively and the decomposition mechanism seems to switch at 409 K.

As in the case of AN, the thermal decomposition process of HNF varies with the temperature of decomposition. Deflagatory decomposition of HNF produces ammonium nitroformate, which decomposes to hydrazine, nitroform, and ammonia.[28] These products react to generate heat in the gas phase and the final combustion products are formed according to:

$$N_2H_5C(NO_2)_3 \rightarrow 2NO + CO_2 + 2H_2O + 3/2N_2 + 1/2H_2$$

The combustion wave structure for HNF consists of two gas-phase zones, similar to that for ADN. However, the melt layer zone observed for ADN is not seen for HNF. The temperature increases rapidly in the gas phase just above the decomposing surface of HNF. It then increases relatively slowly in the first gas-phase zone. It increases rapidly once more at the beginning of the second gas-phase zone, with formation of the final combustion products. Thus, the second reaction zone stands some distance above the decomposing surface of the HNF. The second reaction zone is considered to involve the reaction between the 2NO and $1/2H_2$ produced in the first reaction zone, as represented by

$$2NO + 1/2H_2 \rightarrow N_2 + 1/2H_2O + 3/4O_2$$

This reduction of NO is highly exothermic but relatively slow at low pressure, because it appears to be a third-order reaction, similar to the dark-zone reaction of nitropolymer combustion. The overall reaction of HNF is represented by

$$N_2H_5C(NO_2)_3 \rightarrow CO_2 + 5/2H_2O + 5/2N_2 + 3/4O_2$$

and the adiabatic flame temperature reaches 3120 K. The large number of oxygen molecules formed by the combustion of HNF serve as oxidizers when HNF is mixed with fuel components.

5.2
Combustion of Polymeric Materials

5.2.1
Nitrate Esters

Nitrate esters are either liquid or solid and are characterized by an $O–NO_2$ chemical bond. Typical nitrate esters are nitrocellulose (NC) and nitroglycerin (NG). NC is known as gun cotton, a single-base propellant used for guns. Since NC is a fibrous material, grains are formed by treating it with a solvent. On the other hand, NG is a liquid at room temperature. It is mixed together with NC to form a rubber-like energetic material. This NC/NG mixture is used in explosives and propellants. When this mixture is used for guns and rockets, it is referred to as a double-base propellant.

Extensive experimental and theoretical studies have been performed in an effort to determine the decomposition and combustion processes of nitrate esters. This

subsection provides a summary of the decomposition and combustion mechanisms of various types of nitrate esters presented previously. It is important to acquire sufficient understanding of the governing factors of the combustion of nitrate esters so that the combustion properties encountered during applications can be anticipated. An understanding of the basic steady-state combustion mechanism is a necessary prerequisite for models describing the burning rate as a function of pressure and initial temperature.

5.2.1.1 **Decomposition of Methyl Nitrate**

The simplest nitrate ester is methyl nitrate, which has the chemical structure CH_3ONO_2. The decomposition process is given by:[20,29]

$$\begin{aligned} CH_3ONO_2 &\rightarrow CH_3O^{\cdot} + NO_2 && Q_p = -147 \text{ kJ mol}^{-1} \\ &\rightarrow CH_2O + 1/2H_2 + NO_2 && Q_p = -34 \text{ kJ mol}^{-1} \\ &\rightarrow CO, H_2O, NO, H_2, N_2, N_2O, CH_2O, CO_2 \end{aligned}$$

The first two reaction steps are endothermic; however, the overall reaction is exothermic and the final flame temperature is 1800 K. The observed pressure dependence of the burning rate follows a second-order rate law; the overall activation energy is consistent with the oxidation reaction by NO_2 being the slowest and hence the rate-controlling step.

5.2.1.2 **Decomposition of Ethyl Nitrate**

The primary step in the decomposition of ethyl nitrate ($C_2H_5ONO_2$) is again the breaking of the $C_2H_5O–NO_2$ bond,[30] and the decomposition rate obeys a first-order law. The decomposition process of ethylene glycol dinitrate can be written as:[29]

$$\begin{aligned} \begin{matrix} CH_2ONO_2 \\ | \\ CH_2ONO_2 \end{matrix} &\rightarrow \begin{matrix} CH_2O^{\cdot} \\ | \\ CH_2ONO_2 \end{matrix} + NO_2 && Q_p = -147 \text{ kJ mol}^{-1} \\ &\rightarrow 2CH_2O + NO_2 && Q_p = -113 \text{ kJ mol}^{-1} \end{aligned}$$

The breaking of one $O–NO_2$ bond gives a free radical, which decomposes to formaldehyde and nitrogen dioxide. When butane-2,3-diol dinitrate is decomposed at atmospheric pressure, nitrogen dioxide and acetaldehyde are formed.[31] However, these react rapidly to form nitric oxide within a distance of 2 mm from the decomposing surface. The decomposition of butane-1,4-diol dinitrate produces nitrogen dioxide, formaldehyde, and ethene. A steep temperature increase and a rapid concentration decrease of nitrogen dioxide and formaldehyde are observed within 1 mm of the decomposing surface. It is proposed[31] that the dinitrate decomposes to produce equal amounts of aldehyde and nitrogen dioxide according to:

$$\begin{array}{l} R\text{–}CHONO_2 \\ | \qquad\qquad \rightarrow 2RCHO + 2NO_2 \\ R\text{–}CHONO_2 \end{array}$$

NO_2 is then converted into NO by the oxidation reaction with RCHO.

5.2.1.3 Overall Decomposition Process of Nitrate Esters

As is evident from experimental measurements, most kinds of nitrate esters appear to decompose to NO_2 and C,H,O species with the breaking of the O–NO_2 bond as the initial step. A strong heat release occurs in the gas phase near the decomposing surface due to the reduction of NO_2 to NO accompanied by the oxidation of C,H,O species to H_2O, CO, and CO_2. NO reduction, however, is slow and this reaction is not observed in the decomposition of some nitrate ester systems. Even when the reaction occurs, the heat release does not contribute to the heat feedback to the surface because the reaction occurs at a distance far from the surface.

The decomposition process can be essentially divided into three stages for simple nitrate esters:

Stage 1. $RNO_2 \rightarrow NO_2$ + organic molecules (mainly aldehydes)
Stage 2. NO_2 + intermediate organic products
$\rightarrow$ NO + H_2, CO, CO_2, H_2O, etc., at low pressure
Stage 3. NO + H_2, CO, etc. $\rightarrow$ N_2, CO_2, H_2O, etc. at high pressure
Stage 2 occurs at both high and low pressures.

The decomposition process of double-base propellants is autocatalytic, NO_2 being evolved first and then reacting to increase the rate of its evolution.[32] The first step of the decomposition is the breaking of the RO–NO_2 bond, which is followed by the production of complex organic gases.[33]

Mixtures of HCHO and NO_2 react very rapidly at temperatures above 430 K; NO_2 is reduced almost quantitatively to NO, and the aldehyde is oxidized to CO, CO_2, and H_2O.[34] This process is discussed in detail in Section 5.2.1.4.

5.2.1.4 Gas-Phase Reactions of NO_2 and NO

From the discussion in the previous section, it is clear that, above all, NO_2, and then NO, are the principal oxidizers produced in the flames of nitrate esters. The reaction of NO_2 with aldehydes plays an important role in the combustion of nitrate esters, since these molecules are the major decomposition products of these materials in the first stage of combustion. Pollard and Wyatt studied the combustion process of HCHO/NO_2 mixtures at sub-atmospheric pressures.[34] They found that the reaction occurs very rapidly at temperatures above 433 K, the NO_2 being reduced almost quantitatively to NO, and the aldehyde being oxidized to CO, CO_2, and H_2O. The order of reaction was found to be one with respect to both reactants. The same result has been reported by McDowell and Thomas.[35] The proposed reaction steps are:

$$CH_2O + NO_2 \rightarrow CH_2O_2 + NO$$

$$CH_2O_2 \rightarrow CO + H_2O$$

$$CH_2O_2 + NO_2 \rightarrow CO_2 + H_2O + NO$$

The flame velocity is independent of pressure and the maximum velocity is 1.40 m s^{-1} for a mixture containing 43.2 mol% HCHO. The velocity depends significantly on the mixture ratio; for example, it drops to about half of this value for a mixture containing 60 % HCHO. Powling and Smith measured the flame velocities of CH_3CHO/NO_2 mixtures.[31] The velocity proved to be very sensitive to the CH_3CHO/NO_2 ratio, as Pollard and Wyatt observed for the $HCHO/NO_2$ flame. The velocity is about 0.10 m s^{-1} at 37 % CH_3CHO and decreases to 0.04 m s^{-1} at 60 % CH_3CHO.

The combustion of H_2, CO, and hydrocarbons with NO is important in both the dark zone and the flame zone of nitropolymer propellants. It is well known that NO behaves in a complex way in combustion processes, in that at certain concentrations it may catalyze a reaction to promote a process, while at other concentrations it may inhibit the reaction. Sawyer and Glassman[36] attempted to establish a measurable reaction between H_2 and NO in a flow reactor at 0.1 MPa. Over a wide range of mixture ratios, they found that the reaction did not occur readily below the temperature of NO dissociation, except in the presence of some radicals. Mixtures of CO and NO are also difficult to ignite, and only mixtures rich in NO could be ignited at 1720 K.

Cummings[37] measured the burning velocity of a mixture of NO and H_2 in a burner flame over a wide pressure range, and found it to be independent of pressure (about 0.56 m s^{-1}) between 0.1 MPa and 4.0 MPa. However, Strauss and Edse[38] found that, at a mixture ratio of 1:1, the burning velocity increased from 0.56 m s^{-1} to 0.81 m s^{-1} at 5.2 MPa.

An extensive experimental study on reaction mechanisms involving NO_2 and NO was conducted by Sawyer.[39] He found the reaction of H_2 with NO_2 to be about three times faster than the reaction of H_2 with a 2:1 NO/O_2 mixture, and no reaction was observed between H_2 and NO.

Generally, in calculating the flame speed of a premixed gas, the net reaction is assumed to be second order in the gas phase. However, it is well known that oxidation reactions involving NO are usually termolecular, for example:[40–42]

$$2NO + Cl_2 \rightarrow 2NOCl$$

$$2NO + Br_2 \rightarrow 2NOBr$$

$$2NO + O_2 \rightarrow 2NO_2$$

The experimental results of Hinshelwood and Green[42] tend to support the following mechanism for the reaction between NO and H_2:

$$2NO + H_2 \rightarrow N_2 + H_2O_2 \text{ (slow)}$$

$$H_2O_2 + H_2 \rightarrow 2H_2O \text{ (fast)}$$

The measured order of the overall reaction varies between 2.60 and 2.89. However, Pannetier and Souchay[43] suggested that the above reaction could not be expected to occur owing to the improbable nature of the termolecular process. They proposed

$$2NO \rightleftharpoons N_2O_2 \text{ (fast)}$$

$$N_2O_2 + H_2 \rightarrow N_2 + H_2O_2 \text{ (slow)}$$

$$H_2O_2 + H_2 \rightarrow 2H_2O \text{ (fast)}$$

In the above series of reactions, the slow reaction involving N_2O_2 is the rate-controlling step. The reaction involving NO is fast enough to maintain equilibrium with the N_2O_2. Consequently, it can be seen that the rate of production of N_2 and H_2O is third order with respect to NO and H_2. The overall sum of these reaction steps is indeed third order, while the elementary reactions are all bimolecular, i. e., second order.

In summary, gas-phase reactions between aldehydes and NO_2 occur readily and with strong exothermicity. The rate of reaction is largely dependent on the aldehyde/NO_2 mixture ratio, and is increased with increasing NO_2 concentration for aldehyde-rich mixtures. On the other hand, no appreciable gas-phase reactions involving NO are likely to occur below 1200 K. The overall chemical reaction involving NO appears to be third order, which implies that it is sensitive to pressure. The reactions discussed above are important in understanding the gas-phase reaction mechanisms of nitropolymer propellants.

5.2.2
Glycidyl Azide Polymer (GAP)

5.2.2.1 Thermal Decomposition and Burning Rate

The terminal OH groups of GAP prepolymer are cured with the NCO groups of hexamethylene diisocyanate (HMDI) and crosslinked with trimethylolpropane(TMP) in order to formulate GAP copolymer consisting of 84.8% GAP prepolymer, 12.0% HMDI, and 3.2% TMP, as shown in Fig. 4.8. The thermochemical data for GAP copolymer obtained by differential thermal analysis (DTA) and thermal gravimetry (TG) are shown in Fig. 5.15. The exothermic peak accompanied by mass loss between 475 K and 537 K is attributed to the decomposition and gasification reactions. A two-stage gasification reaction occurs: the first stage occurs rapidly and is accompanied by the evolution of heat, whereas the second stage occurs relatively slowly without the evolution of heat.[44] The activation energy of the first-stage exothermic gasification is 174 kJ mol^{-1}.

A thermally degraded GAP copolymer is produced at 532 K, accompanied by $\beta = 0.25$, where β is the mass fraction loss obtained by thermal degradation.[44] The ex-

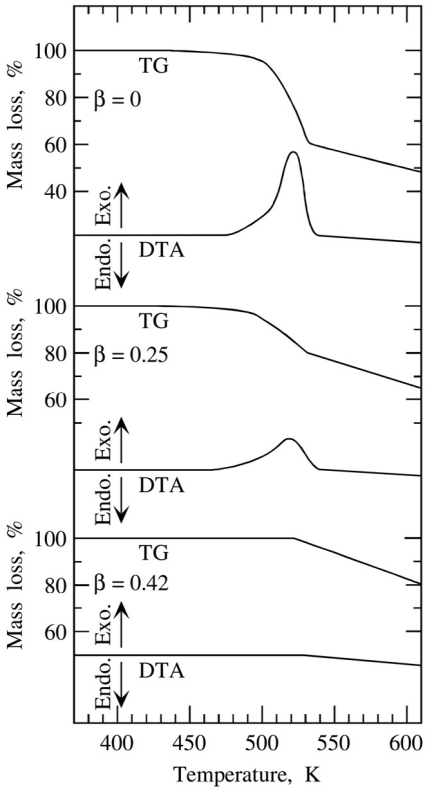

Fig. 5.15 Decomposition of thermally degraded GAP, showing that the exothermic peak decreases as the mass fraction of degradation is increased.

othermic peak is reduced and the first reaction stage, with $\beta = 0.25$, is complete at 529 K, as shown in Fig. 5.15. A thermally degraded GAP copolymer obtained by interruption of the heating at the end of the first reaction stage (537 K, accompanied by $\beta = 0.42$) shows no exothermic peak. The exothermic reaction of GAP copolymer occurs only in the early stages of the decomposition, and no exothermic reaction occurs upon gasification of the remaining mass.

The fraction of nitrogen atoms contained within the GAP copolymer decreases linearly as β increases, as shown in Fig. 5.16. A mass fraction of 0.68 nitrogen atom is present at the first-stage reaction process ($\beta < 0.41$) and the remaining mass fraction of 0.32 nitrogen atoms is gasified in the second-stage reaction process ($\beta > 0.41$). Similar to the loss of the nitrogen atoms, the fractions of hydrogen, carbon, and oxygen atoms within GAP copolymer also decrease linearly as β increases in the region $\beta < 0.41$.

Infrared analysis of GAP copolymer before and after thermal degradation monitored by TG shows that the absorption of the azide bond of the starting GAP copolymer ($\beta = 0.0$) is seen at about $\nu = 2150\ \text{cm}^{-1}$.[44] This azide bond absorption is completely lost following thermal degradation ($\beta = 0.41$). The $-N_3$ bonds within the GAP copolymer decompose thermally above 537 K to produce N_2. Thus, the gasification of the GAP copolymer observed as the first reaction stage occurs due to split-

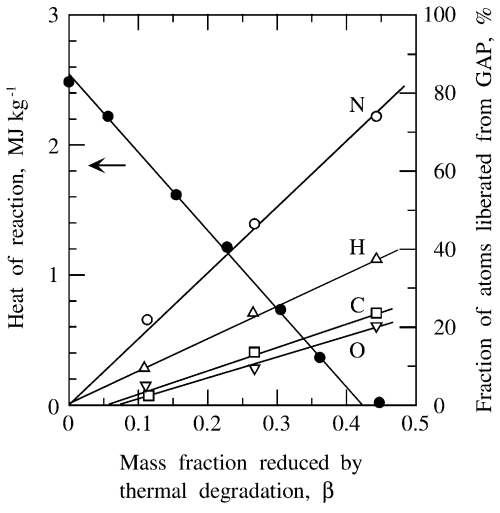

Fig. 5.16 Heat of reaction and fractions of atoms lost from GAP upon thermal degradation.

ting-off of the two nitrogen atoms accompanied by the liberation of heat. The remaining C,H,O molecular fragments decompose at the second reaction stage without the liberation of heat.

The burning rate of GAP copolymer increases linearly with increasing pressure in an ln r versus ln p plot, as shown in Fig. 5.17. The pressure exponent of burning rateat a constant initial temperature, as defined in Eq. (3.71), is 0.44. The temperature sensitivity of burning rate at constant pressure, as defined in Eq. (3.73), is 0.010 K^{-1}.

5.2.2.2 **Combustion Wave Structure**

The combustion wave of GAP copolymer is divided into three zones: zone I is a non-reactive heat-conduction zone, zone II is a condensed-phase reaction zone,

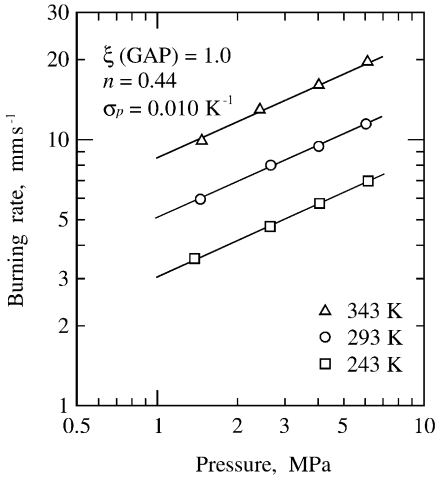

Fig. 5.17 Burning rates of GAP copolymer at three different initial temperatures.

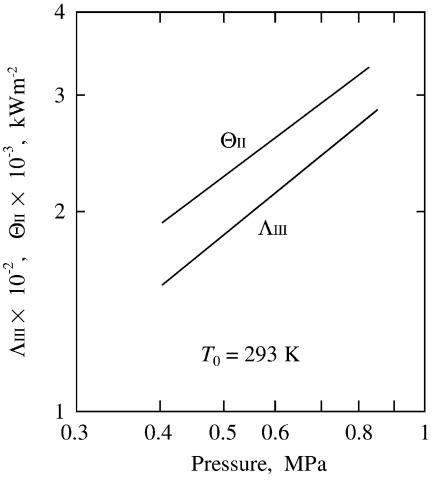

Fig. 5.18 Heat flux transferred back from the gas phase to the burning surface and heat flux produced at the burning surface of GAP copolymer as a function of pressure.

and zone III is a gas-phase reaction zone in which the final combustion products are formed. Decomposition occurs at T_u in zone II, and gasification is complete at T_s in zone II. This reaction scheme is similar to that of HMX or TAGN, as shown in Fig. 5.5.

Using Eqs. (5.1) and (5.2), the heat flux in zone II, Θ_{II}, and the heat flux in zone III (Λ_{III}) are determined from temperature profile data in the combustion wave. As shown in Fig. 5.18, both Θ_{II} and Λ_{III} increase linearly with increasing pressure in a log-log plot: $\Theta_{II} \sim p^{0.75}$ and $\Lambda_{III} \sim p^{0.80}$. The heat of reaction in zone II, Q_{II}, is determined as 624 kJ kg^{-1}.[44] It is noteworthy that the heat of reaction of HMX in zone II is 300 kJ kg^{-1}, even though the adiabatic flame temperature of HMX is 1900 K higher than that of GAP copolymer. Furthermore, Λ_{III} of GAP is of the same order of magnitude as Λ_{III} of HMX, despite the fact that Θ_{II} of GAP is approximately ten times larger than the Θ_{II} of HMX shown in Fig. 5.6.

5.2.3
Bis-azide methyl oxetane (BAMO)

5.2.3.1 Thermal Decomposition and Burning Rate

When BAMO is heated, an exothermic gasification reaction occurs, which is complete when the mass fraction loss reaches 0.35, as shown in Fig. 5.19. During this gasification process, scission of the two azide bonds within BAMO occurs, producing nitrogen gas accompanied by the release of heat.[45] The remaining part continues to gasify without exothermic reaction at higher temperatures. For reference, the thermal decomposition process of BCMO is also shown in Fig. 5.19. No exothermic reaction occurs during the gasification process. Fig. 5.20 shows the decomposition temperature, T_d, and the exothermic peak temperature, T_p, as a function of the heating rate of BAMO. Both T_d and T_p are seen to shift to higher values in an $\ln(\theta/T^2)$ versus $1/T$ plot when the heating rate (θ) is increased. The activation energy associated with the decomposition is 158 kJ mol^{-1}.[30]

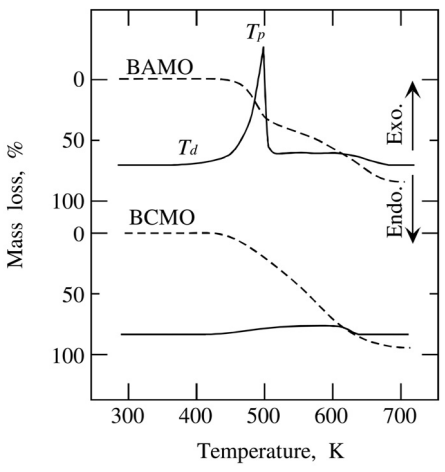

Fig. 5.19 BAMO, containing two C–N_3 bonds, decomposes with rapid heat release accompanied by a mass fraction loss of 0.3. On the other hand, BMCO, containing C–Cl bonds, decomposes relatively smoothly without heat release.

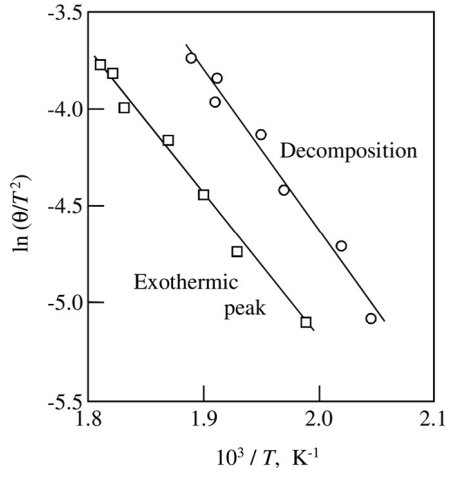

Fig. 5.20 The exothermic peak temperature and decomposition temperature of BAMO shift to higher values as the heating rate is increased.

The heat of decomposition, Q_d, of BAMO copolymer containing different levels of N_3 bond density, $\xi(N_3)$, is shown as a function of $\xi(N_3)$ in Fig. 5.21. BAMO prepolymer is copolymerized with THF. The N_3 bond density is varied by adjusting the mass fraction ratio of BAMO prepolymer and THF.

The relationship between Q_d (MJ kg^{-1}) and $\xi(N_3)$ (mol mg^{-1}) measured by differential scanning calorimetry (DSC) is represented by[46]

$$Q_d = 0.6\xi(N_3) - 2.7 \tag{5.7}$$

The heat of decomposition increases linearly with increasing N_3 bond density.

The condensed-phase reaction zone of a burning-interrupted BAMO copolymer is identified by infrared (IR) spectral analysis. In the non-heated zone, the absorption of the N_3 bond, along with the absorptions of the C–O, C–H, and N–H bonds,

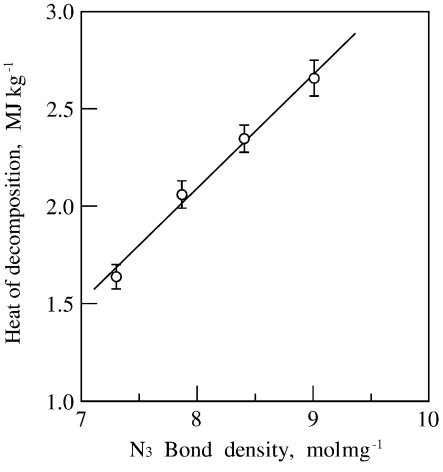

Fig. 5.21 Heat of decomposition increases with increasing N_3 bond density in BAMO copolymer.

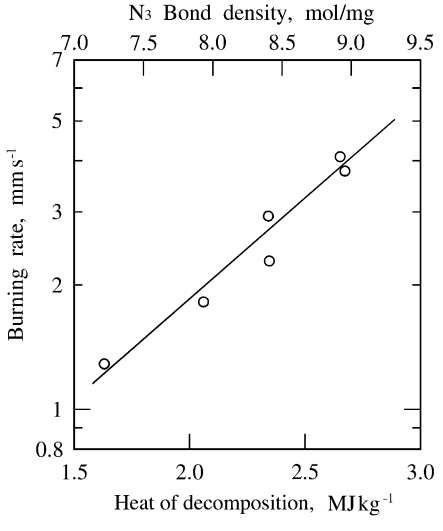

Fig. 5.22 The burning rate of BAMO copolymer increases with increasing heat of decomposition and also with increasing N_3 bond energy.

are seen. In the surface reaction zone (0–0.5 mm below the burning surface), the absorption of the N_3 bond is lost. However, the absorptions of the C–O, C–H, and N–H bonds remain as observed in the non-heated zone. This suggests that an exothermic reaction occurs due to decomposition of the N_3 bonds in the sub-surface and surface reaction zones.[45]

The burning rate of BAMO copolymer at $T_0 = 293$ K is shown as a function of Q_d and $\xi(N_3)$ in Fig. 5.22. The linear dependence of the burning rate, r (mm s^{-1}), in the semi-log plot at 3 MPa is represented by

$$r = 1.84 \times 10^{-4} \exp\,(1.14 Q_d) \tag{5.8}$$

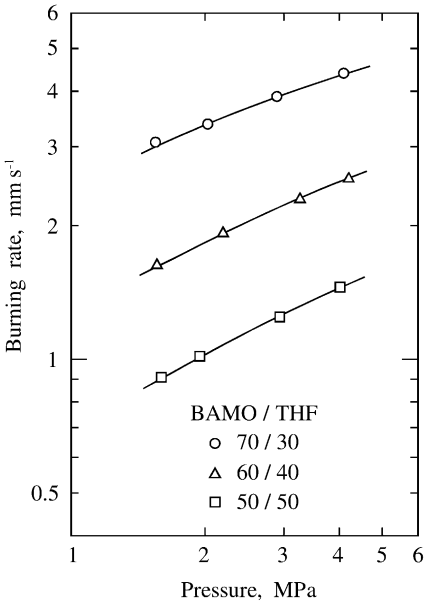

Fig. 5.23 The burning rate of BAMO/THF copolymer increases as the mass fraction of BAMO is increased at constant pressure.

The burning rates of BAMO copolymer samples with the compositions BAMO/THF = 70:30, 60:40, and 50:50 are shown as a function of pressure in Fig. 5.23.[31] The burning rate is seen to increase linearly in an ln r versus ln p plot with increasing pressure at constant T_0. The burning rate is also seen to be highly sensitive to the mixture ratio of BAMO and THF. Furthermore, the burning rate of BAMO copolymer is also sensitive to T_0. For example, the burning rate of BAMO/THF = 60:40 increases drastically when T_0 is increased at constant p, as shown in Fig. 5.24. The burning rate is represented by

$$r = 0.55 \times 10^{-3}\, p^{0.82} \text{ at } T_0 = 243 \text{ K}$$

$$r = 2.20 \times 10^{-3}\, p^{0.61} \text{ at } T_0 = 343 \text{ K}$$

The temperature sensitivity of the burning rate, as defined in Eq. (3.73), is 0.0112 K^{-1} at 3 MPa.

5.2.3.2 **Combustion Wave Structure and Heat Transfer**

During BAMO copolymer burning in a pressurized inert atmosphere, gaseous and carbonaceous solid fragments are formed exothermically at the burning surface. The temperature in the combustion wave of BAMO copolymer increases from the initial value, T_0, to the burning surface temperature, T_s, and then to the flame temperature, T_f. The burning surface temperature of BAMO copolymer with the composition BAMO/THF = 60:40 increases as T_0 increases at constant pressure. For example, at $p = 3$ MPa, $T_s = 700$ K at $T_0 = 243$ K and $T_s = 750$ K at $T_0 = 343$ K. The effect of T_0 on T_s as expressed by $(dT_s/dT_0)_p$ is determined as 0.50.[46]

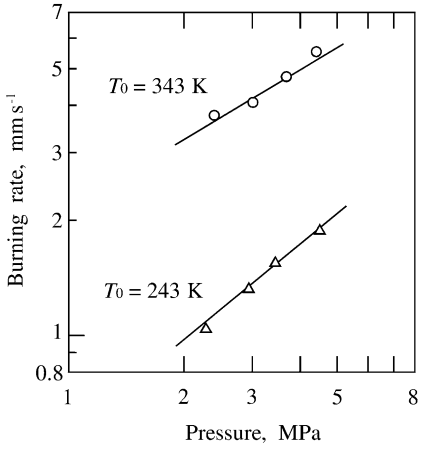

Fig. 5.24 Effect of initial temperature on the burning rate of BAMO/THF = 60:40 copolymer.

As shown in Fig. 5.25, the temperature gradient in the gas phase at $T_0 = 243$ K and $p = 3$ MPa reaches a maximum at the burning surface, decreases with distance from the burning surface, and becomes zero at a distance of about 1.1 mm. When the initial temperature, T_0, is increased from 243 K to 343 K, the temperature gradient is increased and becomes zero at about 0.7 mm from the burning surface.

The energy conservation equation in the gas phase for steady-state burning is given by Eq. (3.41). If one assumes that the physical parameters λ_g and c_g are constant in the gas phase, Eq. (3.14) can be represented by:[46,47]

$$q_d(x) + q_v(x) + q_c(x) = 0 \tag{5.9}$$

$q_d(x) = \lambda_g \, d^2T/dx^2$: heat flux by conduction (5.10)

$q_v(x) = -mc_g \, dT/dx$: heat flux by convection (5.11)

$q_c(x) = Q_g\omega_g(x)$: heat flux by chemical reaction (5.12)

The overall reaction rate in the gas phase $[\omega_g]$ can be represented by

$$[\omega_g] = \int_0^\infty \omega_g(x)dx = m \tag{5.13}$$

Using the burning rate data shown in Fig. 5.24 and the temperature gradient data shown in Fig. 5.25, the heat fluxes given by Eqs. (5.10)–(5.12) can be determined as a function of burning distance. As shown in Fig. 5.25, $q_c(x)$ is maximal at the burning surface and decreases with increasing distance for both low and high initial temperatures.[46] The convective heat flux, $q_c(0)$, at 343 K is 3.3 times higher than that at 243 K, and the reaction distance to complete the gas-phase reaction is 1.1 mm at $T_0 = 243$ K and 0.7 mm at $T_0 = 343$ K. Using the data in Figs. 5.24 and 5.25 and Eq. (5.13), $[\omega_g]$ at 3 MPa is determined as 1.58×10^3 kg m^{-3}s^{-1} at $T_0 = 243$ K and 7.62×10^3 kg m^{-3}s^{-1} at $T_0 = 343$ K.

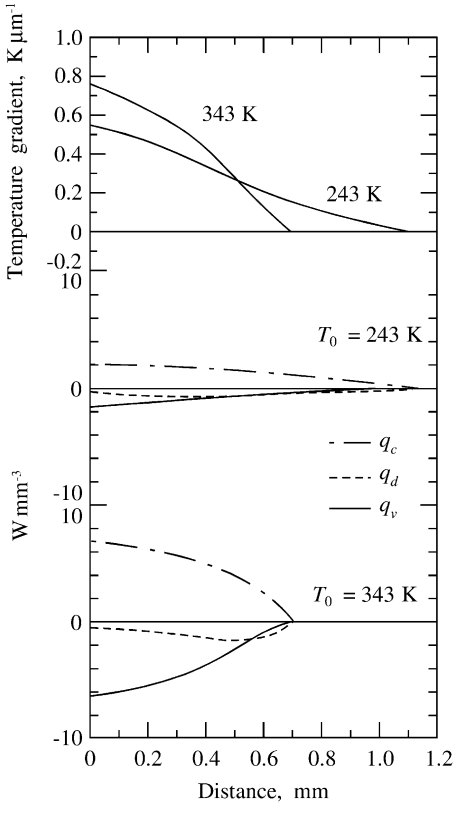

Fig. 5.25 Temperature gradient, conductive heat flux, convective heat flux, and heat flux by chemical reaction as a function of distance from the burning surface at 3 MPa (initial temperatures: 243 K and 343 K) for BAMO/THF = 60:40 copolymer.

Substituting the experimentally derived T_s data into Eqs. (3.75) and (3.76), one obtains:[46]

$Q_s = 457$ kJ kg^{-1} at $T_0 = 243$ K

$Q_s = 537$ kJ kg^{-1} at $T_0 = 343$ K

Substituting the T_s and Q_s data into Eqs. (3.75) and (3.76), the temperature sensitivity of the gas phase, Φ, as defined in Eq. (3.79), and of the solid phase, Ψ, as defined in Eq. (3.80), are determined as 0.0028 K^{-1} and 0.0110 K^{-1}, respectively; Ψ is approximately four times greater than Φ. The computed σ_p represented by the sum of Φ and Ψ is therefore 0.014 K^{-1}, which is approximately equal to the σ_p derived from burning rate experiments. The heat of reaction at the burning surface is the dominant factor on the temperature sensitivity of the burning rate of the BAMO copolymer.

References

1 Arden, E. A., Powling, J., and Smith, W. A. W., Observations on the Burning Rate of Ammonium Perchlorate, *Combustion and Flame*, Vol. 6, No. 1, 1962, pp. 21–33.

2 Levy, J. B., and Friedman, R., Further Studies of Ammonium Perchlorate Deflagration, 8th Symposium (International) on Combustion, The Williams & Wilkins, Baltimore (1962), pp. 663–672.

3 Bircumshaw, L. L., and Newman, B. H., The Thermal Decomposition of Ammonium Perchlorate I, *Proceedings of the Royal Society*, Vol. A227, No. 1168, 1954, pp. 115–132; see also Bircumshaw, L. L., and Newman, B. H., The Thermal Decomposition of Ammonium Perchlorate II, *Proceedings of the Royal Society*, Vol. A227, No. 1169, 1955, pp. 228–241.

4 Jacobs, P. W. M., and Pearson, G. S., Mechanism of the Decomposition of Ammonium Perchlorate, *Combustion and Flame*, Vol. 13, 1969, pp. 419–429.

5 Jacobs, P. W. M., and Whitehead, H. M., Decomposition and Combustion of Ammonium Perchlorate, *Chemical Reviews*, Vol. 69, 1969, pp. 551–590.

6 Jacobs, P. W. M., and Powling, J., The Role of Sublimation in the Combustion of Ammonium Perchlorate Propellants, *Combustion and Flame*, Vol. 13, 1969, pp. 71–81.

7 Hightower, J. D., and Price, E. W., Combustion of Ammonium Perchlorate, 11th Symposium (International) on Combustion, The Combustion Institute, Pittsburgh, PA, 1967, pp. 463–470.

8 Steinz, J. A., Stang, P. L., and Summerfield, M., The Burning Mechanism of Ammonium Perchlorate-Based Composite Solid Propellants, Aerospace and Mechanical Sciences Report No. 830, Princeton University, 1969.

9 Beckstead, M. W., Derr, R. L., and Price, C. F., The Combustion of Solid Monopropellants and Composite Propellants, 13th Symposium (International) on Combustion, The Combustion Institute, Pittsburgh, PA, 1971, pp. 1047–1056.

10 Manelis, G. B., and Strunin, V. A., The Mechanism of Ammonium Perchlorate Burning, *Combustion and Flame*, Vol. 17, 1971, pp. 69–77.

11 Brill, T. B., Brush, P. J., and Patil, D. G., Thermal Decomposition of Energetic Materials 60. Major Reaction Stages of a Simulated Burning Surface of NH_4ClO_4, *Combustion and Flame*, Vol. 94, 1993, pp. 70–76.

12 Mitani, T., and Niioka, T., Double-Flame Structure in AP Combustion, 20th Symposium (International) on Combustion, The Combustion Institute, Pittsburgh, PA (1984), pp. 2043–2049.

13 Guirao, C., and Williams, F. A., A Model for Ammonium Perchlorate Deflagration Between 20 and 100 atm, *AIAA Journal*, Vol. 9, 1971, pp. 1345–1356.

14 Tanaka, M., and Beckstead, M. W., A Three-Phase Combustion Model of Ammonium Perchlorate, AIAA 96–2888, 32nd AIAA Joint Propulsion Conference, AIAA, Reston, VA, 1996.

15 Sarner, S. F., Propellant Chemistry, Reinhold Publishing Corporation, New York (1966).

16 Boggs, T. L., The Thermal Behavior of Cyclotrimethylenetrinitramine (RDX) and Cyclotetramethylenetetranitramine (HMX), Fundamentals of Solid-Propellant Combustion (Eds.: Kuo, K. K., and Summerfield, M.), Progress in Astronautics and Aeronautics, Vol. 90, Chapter 3, AIAA, New York, 1984.

17 Kubota, N., Combustion Mechanism of HMX, *Propellants, Explosives, Pyrotechnics*, Vol. 14, 1989, pp. 6–11.

18 Suryanarayana, B., Graybush, R. J., and Autera, J. R., Thermal Degradation of Secondary Nitramines: A Nitrogen Tracer Study of HMX, *Chemistry and Industry*, Vol. 52, 1967, p. 2177.

19 Kimura, J., and Kubota, N., Thermal Decomposition Process of HMX, *Propellants and Explosives*, Vol. 5, 1980, pp. 1–8.

20 Fifer, R. L., Chemistry of Nitrate Ester and Nitramine Propellants, Fundamentals of Solid-Propellant Combustion (Eds.: Kuo, K. K., and Summerfield, M.), *Progress in Astronautics and Aeronautics*, Vol. 90, Chapter 4, AIAA, New York, 1984.

21 Beal, R. W., and Brill, T. B., Thermal Decomposition of Energetic Materials 77. Behavior of N–N Bridged Bifurazan

Compounds on Slow and Fast Heating, *Propellants, Explosives, Pyrotechnics*, Vol. 25, 2000, pp. 241–246.

22 Beal, R. W., and Brill, T. B., Thermal Decomposition of Energetic Materials 78. Vibrational and Heat of Formation Analysis of Furazans by DFT, *Propellants, Explosives, Pyrotechnics*, Vol. 25, 2000, pp. 247–254.

23 Nedelko, V. V., Chukanov, N. V., Raevskii, A. V., Korsounskii, B. L., Larikova, T. S., Kolesova, O. I., and Volk, F., Comparative Investigation of Thermal Decomposition of Various Modifications of Hexanitrohexaazaisowurtzitane (CL-20), *Propellants, Explosives, Pyrotechnics*, Vol. 25, 2000, pp. 255–259.

24 Häußler, A., Klapötke, T. M., Holl, G., and Kaiser, M., A Combined Experimental and Theoretical Study of HMX (Octogen, Octahydro-1,3,5,7-tetranitro-1,3,5,7-tetrazocine) in the Gas Phase, *Propellants, Explosives, Pyrotechnics*, Vol. 27, 2002, pp. 12–15.

25 Hinshelwood, C. N., The Kinetics of Chemical Change, Oxford University Press, Oxford, 1950.

26 Kubota, N., Hirata, N., and Sakamoto, S., Combustion Mechanism of TAGN, 21st Symposium (International) on Combustion, The Combustion Institute, Pittsburgh, PA, 1986, pp. 1925–1931.

27 Santhosh, G., Venkatachalam, S., Krishnan, K., Catherine, B. K., and Ninan, K. N., Thermal Decomposition Studies on Advanced Oxidiser: Ammonium Dinitramide, Proceedings of the 3rd International Conference on High-Energy Materials, Thiruvananthapuram, India, 2000.

28 Varma, M., Chatterjee, A. K., and Pandey, M., Ecofriendly Propellants and Their Combustion Characteristics, Advances in Solid Propellant Technology, 1st International HEMSI Workshop (Eds.: Varma, M., and Chatterjee, A. K.), Birla Institute of Technology, India, 2002, pp. 144–179.

29 Adams, G. K., and Wiseman, L. A., The Combustion of Double-Base Propellants, Selected Combustion Problems, Butterworth's Scientific Publications, London, 1954, pp. 277–288.

30 Adams, G. K., The Chemistry of Solid Propellant Combustion: Nitrate Esters of Double-Base Systems, Proceedings of the 4th Symposium on Naval Structural Mechanics, Purdue University, Lafayette, IN (1965), pp. 117–147.

31 Powling, J., and Smith, W. A. W., The Combustion of the Butane-2,3- and 4-Diol Dinitrates and Some Aldehyde-Nitrogen Dioxide Mixtures, *Combustion and Flame*, Vol. 2, No.2, 1958, pp. 157–170.

32 Hewkin, D. J., Hicks, J. A., Powling, J., and Watts, H., The Combustion of Nitric Ester-Based Propellants: Ballistic Modification by Lead Compounds, *Combustion Science and Technology*, Vol. 2, 1971, pp. 307–327.

33 Robertson, A. D., and Napper, S. S., The Evolution of Nitrogen Peroxide in the Decomposition of Gun Cotton, *Journal of the Chemical Society*, Vol. 91, 1907, pp. 764–786.

34 Pollard, F. H., and Wyatt, P. M. H., Reactions Between Formaldehyde and Nitrogen Dioxide; Part III, The Determination of Flame Speeds, *Transactions of the Faraday Society*, Vol. 46, No. 328, 1950, pp. 281–289.

35 McDowell, C. A., and Thomas, J. H., Oxidation of Aldehydes in the Gaseous Phase; Part IV. The Mechanism of the Inhibition of the Gaseous Phase Oxidation of Acetaldehyde by Nitrogen Peroxide, *Transactions of the Faraday Society*, Vol. 46, No. 336, 1950, pp. 1030–1039.

36 Sawyer, R. F., and Glassman, I., The Reactions of Hydrogen with Nitrogen Dioxide, Oxygen, and Mixtures of Oxygen and Nitric Oxide, 12th Symposium (International) on Combustion, The Combustion Institute, Pittsburgh, PA, 1969, pp. 469–479.

37 Cummings, G. A. McD., Effect of Pressure on Burning Velocity of Nitric Oxide Flames, *Nature*, No. 4619, May 1958, p. 1327.

38 Strauss, W. A., and Edse, R., Burning Velocity Measurements by the Constant Pressure Bomb Method, 7th Symposium (International) on Combustion, The Combustion Institute, Pittsburgh, 1958, pp. 377–385.

39 Sawyer, R. F., The Homogeneous Gas-Phase Kinetics of Reactions in Hydrazine-Nitrogen Tetraoxide Propellant System, Ph.D. Thesis, Princeton University, 1965.

40 Heath, G. A., and Hirst, R., Some Characteristics of the High-Pressure Combustion of Double-Base Propellants, 8th Symposium (International) on Combustion, Williams & Wilkins Co., Baltimore, 1962, pp. 711–720.

41 Penner, S. S., Chemistry Problems in Jet Propulsion, Pergamon Press, New York, 1957.

42 Hinshelwood, C. N., and Green, T. E., The Interaction of Nitric Oxide and Hydrogen and the Molecular Statistics of Termolecular Gaseous Reactions, *J. Chem. Soc.*, 1926, pp. 730–739.

43 Pannetier, G., and Souchay, P., Chemical Kinetics, Elsevier Publishing Co., New York, 1967.

44 Kubota, N., and Sonobe, T., Combustion Mechanism of Azide Polymer, *Propellants, Explosives, Pyrotechnics*, Vol. 13, 1988, pp. 172–177.

45 Miyazaki, T., and Kubota, N., Energetics of BAMO, *Propellants, Explosives, Pyrotechnics*, Vol. 17, 1992, pp. 5–9.

46 Kubota, N., Combustion of Energetic Azide Polymers, *Journal of Propulsion and Power*, Vol. 11, No. 4, 1995, pp. 677–682.

47 Kubota, N., Propellant Chemistry, *Journal of Pyrotechnics*, 11, 2000, pp. 25–45.